Research

New Phytologist

Network analyses identify a transcriptomic proximodistal prepattern in the maize leaf primordium

Samuel Leiboff[1,2,3]*, Josh Strable[1]*, Robyn Johnston[1]*, Silvia Federici[1], Anne W. Sylvester[1,4] and Michael J. Scanlon[1]

[1]Plant Biology Section, School of Integrative Plant Science, Cornell University, Ithaca, NY 14853, USA; [2]Plant Gene Expression Center, USDA-ARS, Albany, CA 94710, USA; [3]Department of Botany and Plant Pathology, Oregon State University, Corvalis, OR 97331, USA [4]Department of Molecular Biology, University of Wyoming, Laramie, WY 82071, USA

Authors for correspondence:
Anne W. Sylvester
Email: annesyl@uwyo.edu

Michael J. Scanlon
Email: mjs298@cornell.edu

Received: *28 August 2020*
Accepted: *29 November 2020*

New Phytologist (2021) **230:** 218–227
doi: 10.1111/nph.17132

Key words: auricle, boundary, leaf, ligule, maize, network.

Summary

- The formation of developmental boundaries is a common feature of multicellular plants and animals, and impacts the initiation, structure and function of all organs. Maize leaves comprise a proximal sheath that encloses the stem, and a distal photosynthetic blade that projects away from the plant axis. An epidermally derived ligule and a joint-like auricle develop at the blade/sheath boundary of maize leaves. Mutations disturbing the ligule/auricle region disrupt leaf patterning and impact plant architecture, yet it is unclear how this developmental boundary is established.
- Targeted microdissection followed by transcriptomic analyses of young leaf primordia were utilized to construct a co-expression network associated with development of the blade/sheath boundary.
- Evidence is presented for proximodistal gradients of gene expression that establish a prepatterned transcriptomic boundary in young leaf primordia, before the morphological initiation of the blade/sheath boundary in older leaves.
- This work presents a conceptual model for spatiotemporal patterning of proximodistal leaf domains, and provides a rich resource of candidate gene interactions for future investigations of the mechanisms of blade/sheath boundary formation in maize.

Introduction

A key process in plant organogenesis is the specification of developmental boundaries that separate cell and tissue domains in an organ (Hepworth & Pautot, 2015). Maize (*Zea mays* subsp. *mays* L.) leaves are a genetically tractable system to study boundary formation, wherein the ligule/auricle region precisely demarcates the distal blade from the proximal leaf sheath. At this blade/sheath boundary, the epidermally derived ligule fringe emerges from the base of an articulated, joint-like auricle (Fig. 1a,b). Together, the ligule and auricle project the blade away from the main plant axis (Tian *et al.*, 2011). Blade angle is dependent on the geometry and structure of the ligule and auricle region (Sylvester *et al.*, 1990; Kong *et al.*, 2017), and is a major trait under selection during maize domestication and breeding (Tian *et al.*, 2019). The mechanisms that pattern the blade/sheath boundary in the maize leaf remain an open question in plant development.

Maize leaves arise from undifferentiated founder cells encircling the base of the shoot apical meristem (SAM), and emerge sequentially as dorsiventrally flattened primordia that surround the shoot (reviewed by Conklin *et al.*, 2019). The site of an incipient primordium is referred to as Plastochron 0 (i.e. P0, where a plastochron is the time interval between successive leaf initiations (Erickson & Michelini, 1957)) and is associated with downregulation of Class I *KNOTTED1-LIKE HOMEOBOX* (*KNOX*) gene expression (Smith *et al.*, 1992; Jackson *et al.*, 1994; Long *et al*, 1996). As the maize primordium emerges from the SAM periphery, a proximodistal axis forms between the tip of the initiating primordium and its base that surrounds the SAM. In the inbred line B73, the boundary demarcating the future proximal sheath and distal blade becomes morphologically distinct within the sixth and eighth youngest leaf primordia (P6/P8; Fig. 1c–e; Walsh *et al.*, 1998; Johnston *et al.*, 2014). Here, *LIGULELESS1* (*LG1*) transcripts accumulate (Moreno *et al.*, 1997; Johnston *et al.*, 2014) at the ligule/auricle region, and the preligule band forms as a linear field of cells in the adaxial epidermis marked by localized anticlinal cell divisions (i.e. within the plane of the existing cell file; Fig. 1d; Sylvester *et al.*, 1990). Subsequent periclinal divisions (i.e. parallel to the plane) in the adaxial epidermis mark ligule initiation (Fig. 1e) at the blade/sheath boundary.

Molecular genetic analyses of dominant, gain-of-function mutations in a number of class I *KNOX* genes in maize have revealed that ectopic *KNOX* expression generates patches of sheath identity in mutant leaves. This juxtapositioning of sheath

*These authors contributed equally to this work.

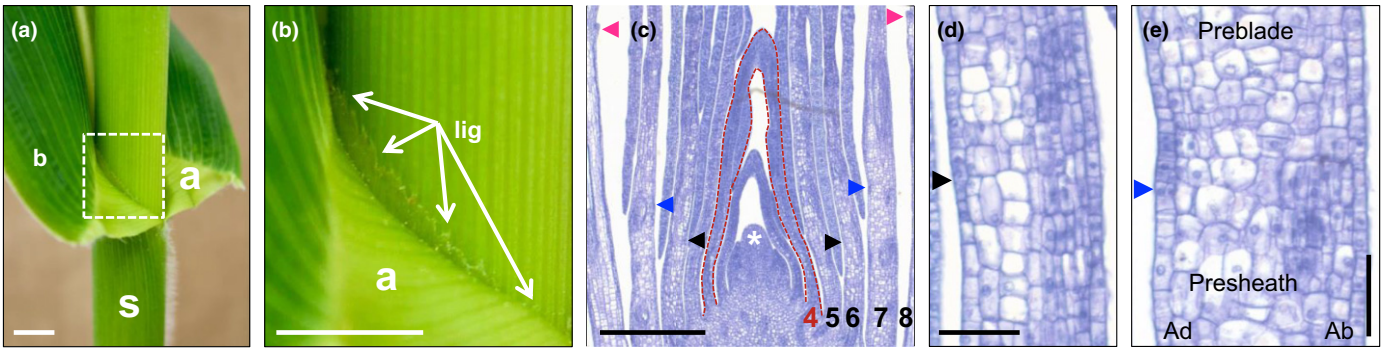

Fig. 1 Morphology and development of the maize blade/sheath boundary. (a) Maize distal blade (b) and proximal stem-surrounding sheath (s) joined at the ligular region (white box) with auricle (a) and ligule (bar,10 mm). (b) Boxed area in (a) of the ligular region consisting of auricle (a) and ligule (l, denoted by arrows) (bar,= 10 mm). (c) Lateral longitudinal section through shoot apex. Numbers indicate plastochron number of leaf primordia. P4 primordium is outlined in red. Asterisk = SAM (bar, 500 μm). (d, e) Enlargement of details in panel (c). (d) is from an adjacent section of the same sample as (c). Arrowheads indicate the preligule band and emerging ligule on successive leaf primordia. Black arrowheads denote the preligule band is first visible at P6. Blue arrowheads denote periclinal division of preligule band cells in the adaxial epidermis at P7. Magenta arrowheads indicate the initiating ligule on the adaxial side of the leaf at P8. Ad, adaxial; Ab, abaxial; bars, 50 μm.

tissue within what is normally blade coincides with the *de novo* formation of ligule/auricle structures at these ectopic blade/sheath boundaries in *Knox* mutant leaves (Smith *et al.*, 1992; Jackson *et al.*, 1994; Freeling & Hake, 1985; Becraft & Freeling, 1994; Schneeberger *et al.*, 1995; Muehlbauer et al., 1997, 1999; Foster *et al.*, 1999). These mutant phenotypes highlight a critical role for *KNOX* regulatory networks in specifying proximal developmental cues in developing leaf primordia (reviewed by Bolduc *et al.*, 2012a).

Previously, we used laser microdissection followed by RNA sequencing (LM-RNAseq) to identify genes expressed in the initiating ligule/auricle region (Johnston *et al.*, 2014). Precise regions of preligule, preblade and presheath were microdissected from P7-staged leaf primordia, revealing that significant numbers of transcripts that are differentially expressed at the developing blade/sheath boundary are also expressed at multiple organ boundaries. Thus, genes expressed during maize ligule/auricle initiation recapitulate gene expression patterns that occur during lateral organ initiation throughout shoot development (Johnston *et al.*, 2014). Moreover, genes known to be bound and modulated by KNOTTED1 (KN1; Bolduc *et al.*, 2012b) are over-represented during ligule initiation (Johnston *et al.*, 2014), further implicating KNOX gene networks in patterning the blade/sheath boundary. Intriguingly, several transcripts that preferentially accumulate at the initiating ligule/auricle region of P7-staged leaf primordia are likewise expressed at the base of much younger, P4-staged leaves, long before any evidence of ligule/auricle morphogenesis (Johnston *et al.*, 2014).

We use the term 'prepattern' here to describe gradients of gene expression within a tissue or organ that contribute to eventual developmental patterning, which are present before any evidence of morphological changes that define this pattern (reviewed by Van Norman *et al.*, 2013; Lim *et al.*, 2017). In this study, network analyses provide evidence for transcriptional gradients along the proximodistal axis of P4-staged leaves that establish a prepatterned boundary of gene expression in young leaf primordia, before the morphological initiation of the blade/sheath boundary in older leaves.

Materials and Methods

Genetic stocks and plant growth

Maize plants were grown in field U at the Cornell Musgrave Research Farm (Lima silt loam soil), Cornell Guterman Greenhouse (conditions: 29.4°C : 23.9°C, day : night, 16 h : 8 h light : dark; soil type: 1 : 1 Turface MVP (Profile Products LLC, Buffalo Grove, IL, USA) : LM111 (Lambert Peat Moss, QC, Canada)) and Cornell Weill Hall Plant Growth Chamber Lab (conditions: 29.4°C : 23.9°C, day : night, relative humidity 50%, 16 h : 8 h, light : dark, light intensity of 514 μmol at plant height; soil type: 1 : 1 Turface MVP (Profile Products LLC) : LM111 (Lambert Peat Moss)). The *Kn1-DL* allele (Ramirez *et al.*, 2009; backcrossed eight generations into the B73 inbred line) was obtained from M. Muszynski (University of Hawai'i at Mānoa). Homozygous *lg2-R* plants introgressed into the B73 background and wild-type siblings (described by Walsh *et al.*, 1998) were used for LM-RNAseq analysis of *lg2* mutants.

RNA *in situ* hybridization and immunohistolocalization

Shoot apices from glasshouse-grown 2-wk-old seedlings were fixed overnight at 4°C in FAA (3.7% formalin, 5% glacial acetic acid and 50% ethanol in water). Tissues were dehydrated at 4°C through a graded ethanol series (50%, 70%, 85%, 95%, 100%) each for 1 h, with three changes in 100% ethanol, and kept in 100% ethanol at 4°C overnight. Tissues were then passed through a graded Histo-Clear (National Diagnostics, Atlanta, GA, USA) series (3 : 1, 1 : 1, 1 : 3 ethanol : Histo-Clear) with three changes in 100% Histo-Clear; all changes were 1 h each at room temperature. Samples were then embedded in Paraplast Plus (McCormick Scientific, St Louis, MO, USA), sectioned and hybridized with probes synthesized as described previously

(Jackson *et al.*, 1994). Hybridizations were performed using antisense digoxygenin-labeled RNA probes: *ZHD15* (JS131, GAGTTCGCGGAGAAGCAGG; JS132, GATATGCCACCC GTGACACG), *IG1* (JS117, AAAGGAGGCCGAATTCCAGC; JS118, GTAGGCGAGGGAGTTCACG), *GLU1* (JS105, ACT TTGAATGGTTTGCCGGC; JS106, CAACGCGTTATTA GCCACGG; JS017, ACGTACGTGTATCAGAGACATGG; JS108, CGAAGGTGAAGTCAGAGGGG) and *DHN13* (JS396, TCCGATTGGCCTTCCATTCC; JS397, CAGATCTCAGT CGCTGTCGC). Immunohistolocalizations using an anti-KN1 antibody were performed as described by Bolduc *et al.* (2012b).

Histology

Toluidine Blue O (TBO) staining was performed as described by Ruzin (1999) on maize shoot apices from glasshouse-grown 2-wk-old seedlings with the following modification: slides were stained in 0.5% TBO staining solution for 1 min.

Laser microdissection, library preparation and sequencing

Seedling shoot apices were fixed and processed for LM, and sectioned along the lateral axis (Johnston *et al.*, 2014, 2017). LM-RNAseq was conducted to identify genes that are differentially expressed along the proximodistal axis of P4 leaf primordia. Five measured domains of B73 P4 leaf primordia were microdissected (Fig. 2a; Supporting information Fig. S1). These domains encompassed cells that would give rise to the sheath, ligule and proximal part of the blade, although no morphological markers are present at the P4 stage. Domain A was a triangular segment at the very base of the primordium, with the proximal boundary at the insertion point of the leaf and the distal boundary perpendicular to the leaf surface. B, C and D were consecutive 50 µm domains distal to the A domain. E was a 50 µm domain 100 µm distal to the D domain. We collected three replicates of five plants each (for a total of 15 plants), and the three median sections from each shoot apex were used.

LM-RNAseq was conducted to identify genes that are DE in leaf primordia of *lg2-R* mutants and wild-type siblings. LM was used to isolate tissue from regions of P4, P6 and P7 primordia that encompass cells where the blade/sheath boundary will form. The regions captured were the proximal 150 µm of P4, between 200 and 1000 µm from the base of P6, and between 1000 and 3000 µm from the base of P7, as shown in Fig. S2.

LM was performed using the Positioning and Ablation with Laser Microbeams system (PALM Microlaser Technologies, Jena, Germany). RNA extraction and amplification and cDNA library preparation were performed as described previously (Johnston *et al.*, 2014). RNA amplification for *lg2-R* was performed according to the manufacturer's instructions using the TargetAmp 2-Round Aminoallyl-aRNA Amplification Kit 1.0 (Epicentre Biotechnologies, Madison, WI, USA) for wild-type replicates 1 and 2 for P4, P6 and P7 samples and Arcturus RiboAmp HS Plus Kit (ThermoFisher Scientific, Waltham, MA, USA) for nonmutant replicates 3 and 4, and all *lg2-R* replicates for P4, P6 and P7 samples. Illumina sequencing was done on a HiSeq2500.

RNAseq alignment, counting and normalization

Sequence quality was evaluated using FastQC v.0.11.8 (Andrews, 2010) and MultiQC v.1.7 (Ewels *et al.*, 2016). Illumina adapter sequences were trimmed using Trimmomatic v0.39 (Bolger *et al.*, 2014). Reads were aligned to the maize B73 AGPv3.30 genome using TopHat v.2.1.0 (with options -r 0 -i 30 -I 100000; Kim *et al.*, 2013). Aligned reads were counted using a union-exon approach with HTseq-Counts v.0.9.1 (Anders *et al.*, 2015) to the B73 AGPv3.30 gene set. Pairwise hypothesis testing was conducted in DESeq2 (Anders & Huber, 2012) and batch-corrected for principal components analysis (PCA) using Limma (Ritchie *et al.*, 2015). Samples were evaluated for overall quality using a Pearson correlation distance matrix. Raw counts were normalized using the R package edgeR v.3.20.9 and fit to ANOVA-like models using bioreplicate and microdomain as factors (Robinson *et al.*, 2010; McCarthy *et al.*, 2012). Genes with < 5 reads per million were not considered in subsequent analysis.

Self-organizing map analysis

We clustered the normalized, z-scaled expression values from 1045 P4 responsive genes by self-organizing maps into a 5×5 hexagonal grid with 50 000 iterative steps and a learning rate of $a = 0.15$ with R/kohonen v.3.0.7 (Wehrens & Buydens, 2007; Wehrens & Kruisselbrink, 2018). To confirm that we identified all major expression patterns in the dataset, we empirically determined 5×5 to be the largest set of nodes possible that did not yield empty nodes. To find putative KN1 target genes in P4 microdomains, the list of 1045 differentially expressed genes (DEGs) across microdomains A–D was compared with KN1 bound or KN1 bound and modulated genes as classified by Bolduc *et al.* (2012b: Supplemental Table 11 therein).

Weighted gene co-expression network analysis

We used R/wgcna v.1.66 (Langfelder & Horvath, 2008, 2012) to estimate co-expression networks on a Pearson-correlation distance matrix. We empirically determined 32 as an optimal soft-threshold for scale-free topology and maximal connectivity. We used a minimum module size of 50 to allow for highly specialized co-expression patterns. Networks were exported and visualized using Cytoscape (Shannon *et al.*, 2003).

Data access

P4 domain RNAseq reads will be available to download from the NCBI SRA under BioProject no. PRJNA565780. RNAseq reads for *liguless2-R* vs wild-type leaf primordia will be available to download from the NCBI SRA under BioProject no. PRJNA625526.

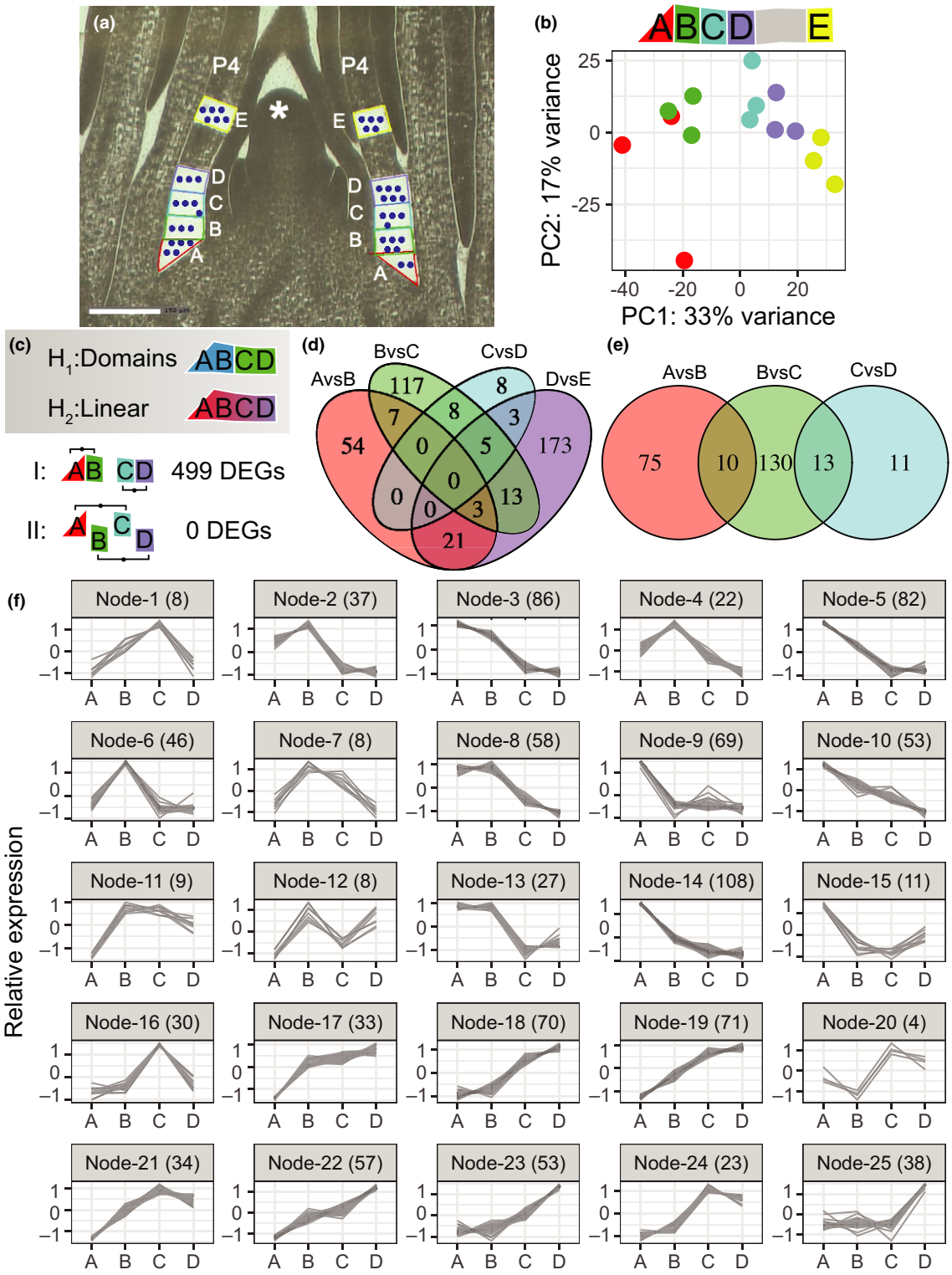

Fig. 2 LM-RNAseq of the base of P4 primordia uncovers abrupt transcriptional shifts along the first 200 μm of the proximodistal axis. (a) Median lateral section through maize shoot apex after P4 laser microdissection. Five 50 μm tall domains collected along the proximodistal axis (microdomains A–E) by UV laser dissection and catapult (blue dots). Asterisk, shoot apical meristem (SAM); bar,150 μm. (b) Batch-corrected expression data from leaf domains (upper) separated into two clusters by PCA (lower), AB and CDE. (c) To evaluate whether the data support the presence of discrete domains (H_1) or continuous linear changes in gene expression across A–D (H_2), signatures of differentially expressed genes (DEGs) were compared between AB vs CD (I) and AC vs BD (II). (d) DEG overlap for neighboring tissue microdomains reveals the highest number of unique transcriptional differences between B vs C and D vs E (Adj $P < 0.05$). (e) DEG overlap for only contiguous tissue microdomains A–D shows the highest number of unique transcriptional differences for B vs C (Adj $P < 0.05$). (f) Normalized AD domain transcript patterns separated into 25 expression patterns by self-organizing maps. Gray lines denote individual transcript accumulation patterns. Labels denote the node IDs, with the number of genes per node in parentheses.

Accession numbers

Specific genes analyzed in this study: *KN1*, GRMZM2G017087; *ZHD15*, GRMZM2G089619; *ZHD1*, GRMZM2G068330; *ZHD21*, GRMZM5G821755; *IG1*, GRMZM2G118250; *TRU1*, GRMZM2G039867; *TRL1*, GRMZM2G060723; *ZmBOPa*, GRMZM2G026556; *ZmBOPb*, GRMZM2G022606; *GLU1*, GRMZM2G016890; *DHN13*, GRMZM2G169372.

Results and Discussion

Gene-expression gradients in the P4-staged maize leaf primordium

LM-RNAseq was used to profile gene expression at the base of P4-staged leaf primordia (Fig. 2a), and search for evidence of transcriptional gradients marking early proximodistal patterning events in developing maize leaves. The base of the P4 primordium was precisely laser-microdissected in four contiguous *c.* 50 μm tissue segments (named microdomains A–D) and an equivalent sized distal segment (microdomain E; Fig. 2a; Fig. S3a,b). Amongst the 21 000 gene models confidently expressed in all samples, a total of 1984 DEGs were identified across all leaf microdomains (Dataset S1). Hierarchical clustering of the transcripts identified a distinction between the two most proximal (A and B) and three distal (C, D and E) microdomains (Fig. S3c). The transcript accumulation patterns of previously described genes (including *ZmCUC2*, *TRU1*, *AUXIN RESPONSE FACTOR24*, *BLH14* and *UNKNOWN*) within specific P4 microdomains were consistent with published *in situ* hybridization data (Fig. S3d) (Johnston *et al.*, 2014).

After batch correction to remove bioreplicate effects, PCA on the top 15 000 most variant transcripts identified a continuous transcriptional gradient amongst samples that followed their proximodistal position from A to E, although a pronounced separation between B and C microdomain samples suggested a large transcriptional shift between the groupings of proximal AB and distal CDE microdomains (Fig. 2b).

Two pairwise gene expression comparisons were performed to determine whether this transcriptional gradient could be attributed to the early patterning (i.e. prepatterning) of microdomains comprising the future blade/sheath boundary (Fig. 2c, hypothesis 'H_1'), or to an intrinsic, linear change across microdomains A–D that reflects proximodistal cell maturation (Fig. 2c, hypothesis 'H_2'). We reasoned that comparing A&B to C&D samples should reveal *both* domain-specific ('H_1') and linearly changed ('H_2') expression patterns, but scrambled comparisons of A&C to B&D samples should reveal only linearly changed ('H_2') expression patterns, as the modeled average of A&C and B&D will still occupy distinct positions along a proximodistal axis. Comparisons of microdomains A&B to C&D yielded 499 DEGs, while the A&C to B&D comparison yielded no DEGs (Datasets S2, S3). We further reasoned that domain identity should involve unique gene regulation patterns when comparing across domains while linearly changed genes may be differentially regulated in multiple domains. We therefore determined DEGs by comparing all neighboring microdomains: A vs B – 85 DEGs (Dataset S4), B vs C – 153 DEGs (Dataset S5), C vs D – 24 DEGs (Dataset S6) and D. vs E – 218 DEGs (Dataset S7). The unique DEGs in these comparisons identified large transcriptomic differences in the B vs C and D vs E comparisons (Fig. 2d): A vs B – 54 unique DEGs (64%; Dataset S8), B vs C – 117 unique DEGs (76%; Dataset S9), C vs D – eight unique DEGs (33%; Dataset S10) and D vs E – 173 unique DEGs (81%; Dataset S11). Microdomain E was collected from a distal tissue that is not contiguous with all other domains A–D, so we wondered if comparing against E was biasing our ability to detect subtle patterns. Limiting our comparisons to unique DEGs between A vs B, B vs C and C vs D only, we similarly found that B vs C contains the largest number of unique DEGs (130; Fig. 2e). Interestingly, we found that A vs B, B vs C and C vs D contained no shared DEGs found in all three of these comparisons, which does not support a linear change in gene expression across these domains. Thus, these analyses reveal a proximodistal, transcriptomic boundary at the base of P4 leaf primordia, before detection of any morphological changes within or between these leaf microdomains. We hypothesize that these dramatic domain-specific differences in transcript accumulation comprise a proximodistal prepattern within P4 leaf primordia, wherein microdomains A&B will form sheath and C,D&E will form blade during later stages of leaf development.

Candidate genes and gene networks implicated in prepatterning proximodistal leaf programs were identified by categorizing the patterns of transcript accumulation across P4 leaf microdomains. Limiting the analysis to DEGs within the four contiguous P4 microdomains A–D, 1045 transcripts were identified (Dataset S12). Unsupervised machine learning separated expression patterns across P4 microdomains for these 1045 DEGs into a self-organizing map comprising a maximum of 25 expression nodes and corresponding expression patterns (Fig. 2f). Several classes of expression patterns were detected, including: linear proximodistal gradients (e.g. Nodes 10 and 22); proximodistal on/off switches (e.g. Nodes 2 and 13); microdomain-specific spikes (e.g. Nodes 6, 9, 16 and 25); and other profiles. As described in our pairwise gene expression analysis, 19 of the 25 nodes (i.e. Nodes 1–8; 10, 12–14, 16, 18–21 and 23–24) reflected particularly dynamic changes in gene expression between microdomains B and C, including 378 transcripts (*c.* 36.2%) with higher accumulation in microdomains A&B vs 282 transcripts (*c.* 27%) with higher accumulation in domains C&D (Fig. 2f; Datasets S13 and S14). These transcriptomic data identify an expression boundary between P4 microdomains AB and CD that precedes, and may predict, proximodistal patterning of the blade–sheath boundary of the maize leaf, supporting the hypothesis of a prepattern at the base of the primordium.

A role for KNOX gene expression networks in proximodistal patterning of maize leaves

The list of genes that are differentially expressed in P4 microdomains is significantly enriched for predicted transcription factors (14.4%; 151/1045; χ^2 $P = 9.86 \times 10^{-17}$; Dataset

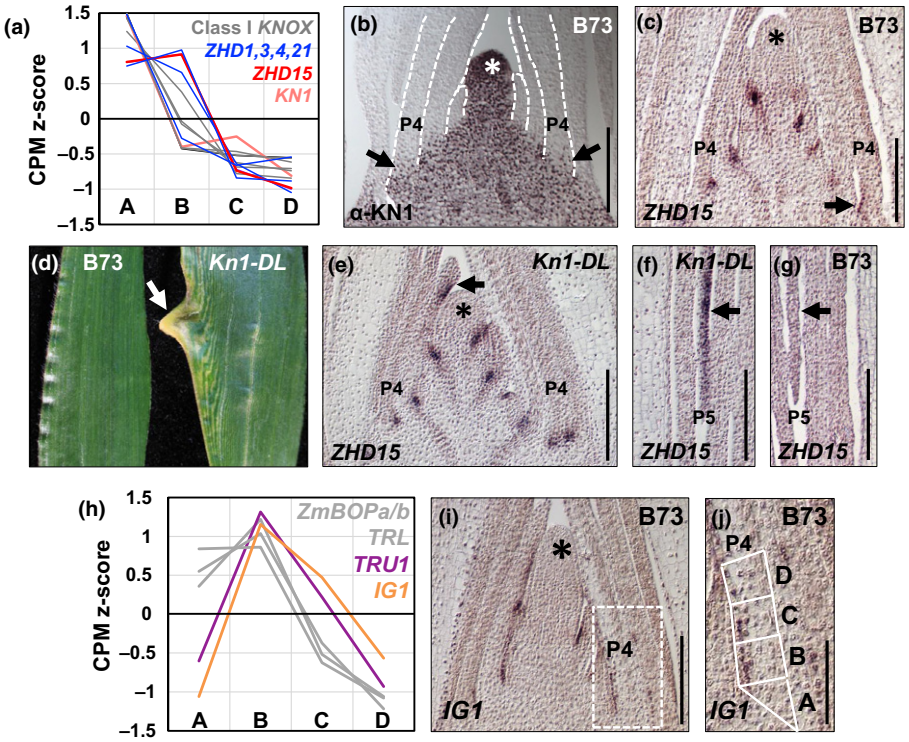

Fig. 3 Accumulation of *KNOX*, *ZHD*, *BOP* and *IG1* gene products during proximodistal development of maize leaf primordia. (a) Transcript profiles of class I *KNOX* and *ZHD* genes (which are direct targets of KN1) reveal co-expression and enrichment in AB domains. (b) Immunostaining of KN1 in a lateral longitudinal section of the B73 shoot apex. Arrows point to KN1 accumulation in the proximal region of the P4 primordium (bar, 200 μm). (c) Median longitudinal section through B73 shoot apex hybridized with *ZHD15* antisense RNA probe. Arrow indicates adaxial accumulation in equivalent AB domains (bar, 200 μm). (d) Normal sibling and *Kn1-DL* leaf margin. Arrow indicates marginal outgrowth of sheath-like tissue. (e) Median longitudinal section through *Kn1-DL* shoot apex hybridized with *ZHD15* probe. Arrow indicates ectopic accumulation of *ZHD15* transcripts (bar, 200 μm). (f) Longitudinal section through *Kn1-DL* P5 leaf margin hybridized with *ZHD15* probe. Arrow points to margin cells with ectopic accumulation of *ZHD15* transcripts. (g) Longitudinal section through B73 P5 leaf margin hybridized with *ZHD15* probe. Arrow points to margin cells with no ectopic accumulation of *ZHD15* transcripts (bar, 200 μm). (h) Co-expression of the *BOP* homologs *TRU1/TRL1/ZmBOPa/b* and of *IG1* in AB domains. (i) Median longitudinal section through B73 shoot apex hybridized with *IG1* antisense RNA probe. (j) Boxed area of (i), showing close-up of proximal region of P4 primordium (bar, 200 μm). (b, c, e, i) Asterisk, shoot apical meristem (SAM).

S15). In particular, microdomain A, at the base of the P4 primordium, was enriched for transcripts from predicted homeobox genes (14.3%; 19/133; χ^2 $P = 1.03 \times 10^{-20}$; Dataset S15), including the Class I *KNOX* genes *KN1*, *RS1*, *GN1*, *LG3*, *LG4*, *KNOX5* and *KNOX8* (Fig. 3a). *KN1* transcripts accumulate at the base of primordia (Fig. 3a; Bolduc & Hake, 2009), while KN1 protein is detected in microdomain B as well as microdomain A (Fig. 3b). These data suggest that KN1 protein moves from microdomain A into B, consistent with its reported cell-to-cell trafficking in the maize shoot (Jackson, 2002). Additionally, a significant number of P4 DEGs are direct transcriptional targets of KN1 (17%; 178/1045; χ^2 $P = 3.08 \times 10^{-196}$; Datasets S15 and S16; Bolduc & Hake, 2009), the majority of which are more highly expressed in proximal P4 microdomains A&B (i.e. Nodes 3, 5, 8 and 14; Fig. 2f). Misexpression of maize KNOX genes in the leaf blade conditions the development of ectopic sheath and ligule tissue in the leaf blade. It is hypothesized that KNOX signaling patterns sheath identity, and that ectopic auricle and ligule form *de novo* at the boundaries where blade and sheath tissues are juxtaposed in *KNOX* mutant leaves (reviewed by Bolduc *et al.*, 2012a).

Notably, the sheath is the last part of the leaf primordium to emerge from the SAM and is the last to elongate in wild-type maize; therefore, it is predicted that the sheath domain occupies a small zone at the base of the P4 leaf primordium (Poethig, 1984; Poethig & Szymkowiak, 1995). This developmental pattern is consistent with our findings of microdomain-specific transcript profiles at the base of the P4 (Fig. 2). We hypothesize that KNOX function specifically prepatterns sheath identity in the proximal P4 microdomains A&B, before any morphological or anatomical differentiation of sheath and/or blade tissue. We further propose that KNOX-mediated sheath cell identity persists at later stages of development when KNOX genes are no longer expressed in the sheath domain (reviewed by Bolduc *et al.*, 2012a; Johnston *et al.*, 2014).

To investigate putative developmental pathways acting downstream of *KNOX* genes during leaf proximal–distal patterning, we analyzed KN1-target genes that are differentially expressed in P4 leaf primordium microdomains. Transcripts from five members of the *ZINCFINGER HOMEODOMAIN* (*ZHD*) gene family, a class of putative transcriptional regulators (Tan & Irish, 2006; Hu *et al.*, 2008) previously undescribed in maize, were

upregulated in P4 microdomains A&B; this pattern was similar to the pattern of KN1 protein accumulation (Fig. 3a). Moreover, *ZHD1*, *ZHD4*, *ZHD15* and *ZHD21* are direct gene targets of KN1 (Fig. S4; Bolduc *et al.*, 2012b). *In situ* hybridization analyses confirm the accumulation of *ZHD15* transcripts at organ boundaries and in the proximal A&B microdomains of P4-staged leaf primordia (Fig. 3c).

Accumulation of *ZHD15* transcripts was examined in the dominant *Kn1-DL* mutant, which produces ectopic outgrowths of sheath and ligule along the blade margin (Fig. 3d; Ramirez *et al.*, 2009). We hypothesized that if KN1 regulates expression of ZHD genes, then the misexpression of KN1 in gain-of-function mutants should lead to misexpression of its gene targets. Indeed, *ZHD15* transcripts accumulate abnormally in the developing leaf margins of *Kn1-DL* mutants, in regions corresponding to the initiation of ectopic sheath outgrowths (Fig. 3e–g). These results suggest that KN1 activity leads to *de novo* expression of *ZHD15* during the formation of ectopic blade/sheath boundaries in *Kn1-DL* mutant leaf blades. Intriguingly, maize *ZHD* genes are also expressed in P7 leaf primordia during ligule initiation (Johnston *et al.*, 2014), as well as in P4 proximal microdomains A&B. Together, these data suggest that maize ZHDs may function downstream of KN1 during maize leaf development.

Our LM-RNAseq data identified steep gradients of differential gene expression between P4 microdomains B and C (Fig. 2c,d). We analyzed five genes that have relatively high expression in P4 microdomain B and decreased or no accumulation in microdomain C (Fig. 3h). These include four maize homologs of Arabidopsis *BOP1/2* (i.e. *TASSELS REPLACE UPPER EARS1* (*TRU1*; Dong *et al.*, 2017), *TRU1-LIKE1* (*TRL1*), *BLADE-ON-PETIOLEa* (*ZmBOPa*) and *ZmBOPb*) and *INDETERMINANT GAMETOPHYTE1* (*IG1*; Evans, 2007), the maize homolog of *Arabidopsis ASYMMETRIC LEAVES2* (*AS2*; Iwakawa *et al.*, 2002). *In situ* hybridizations confirm the accumulation of *IG1* transcripts in the adaxial epidermis of microdomain B in P4 primordia (Fig. 3i,j). Previously described mutations in *IG1* disrupt ligule/auricle patterning and *ig1* mutant leaves misexpress *KNOX* genes (Evans, 2007), consistent with the reported role of AS1/AS2 as a repressor of *KNOX* expression in leaf primordia (Lodha *et al.*, 2013). The maize *BOP* homolog *TRU1* is bound-and-modulated by KN1 (Fig. S5; Bolduc *et al.*, 2012b). In Arabidopsis, BOP1 directly targets and activates expression of *AS2* in proximal, adaxial regions of developing leaf primordia (Jun *et al.*, 2010). We hypothesize a similar interaction in maize, where TRU1 activates expression of *IG1* during specification of the blade/sheath boundary.

Co-expression network yields insight into ligule/auricle patterning

A weighted gene co-expression network analysis (WGCNA; Langfelder & Horvath, 2008) was constructed that incorporated the data derived from 61 LM-RNAseq libraries from P4 (this study) and P7 primordia (Johnston *et al.*, 2014) from the inbred line B73, P6 primordia data from *lg1-R* mutants that form disrupted blade/sheath boundaries, and nonmutant siblings (Johnston *et al.*, 2014), and P4, P6 and P7 data from *lg2-R* mutants and nonmutant siblings (this study). This approach enabled the classification of 23 912 gene transcripts (Fig. 4a; Dataset S17), recapturing and supporting several of the gene expression nodes and RNA *in situ* hybridization patterns described in Figs 2 and 3. For example, Class I *KNOX* genes *KN1*, *GN1*, *RS1*, *LG3*, *LG4*, *KNOX5* and *KNOX8* reside in a module along with 1370 co-expressed genes, of which 170 were identified previously as KN1

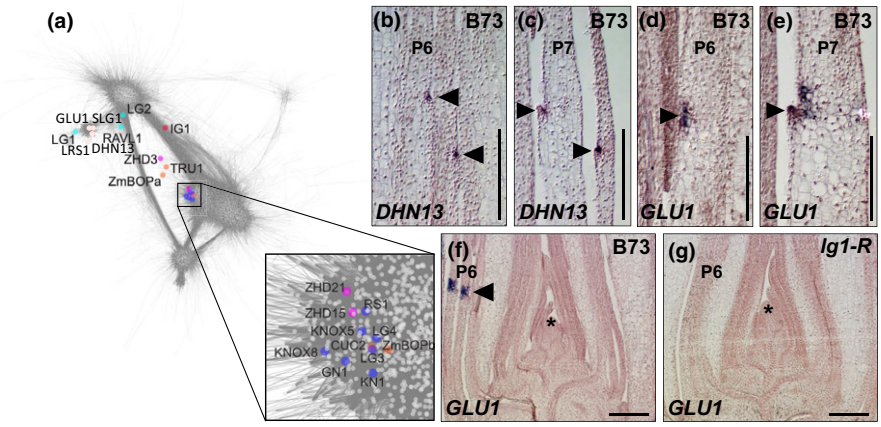

Fig. 4 Co-expression network analysis predicts gene functional interactions during proximodistal development of maize leaf primordia. (a) WGCNA of 61 leaf primordia LM-RNAseq libraries. Cyan module with *LG1*, *LG2* and *RAVL1* known ligule/auricle patterning genes cluster with late expressed genes *GLU1*, *DHN13*, *SLG1* and *LRS1* (mistyrose module). Early patterning genes from the *KNOX* (blue), *TRU1/ZmBOP* (orange), *IG1* (red) and *ZHD* (pink) modules cluster together. (b, c) Longitudinal section through B73 leaf primordia P6 (b) and P7 (c) hybridized with *DHN13* antisense RNA probe. Arrowhead indicates adaxial accumulation in ligule/auricle region (bar, 200 μm). (d, e) Longitudinal section through B73 leaf primordia P6 (d) and P7 (e) hybridized with *GLU1* antisense RNA probe. Arrowhead indicates adaxial accumulation in ligule/auricle region (bar, 200 μm). (f) Longitudinal section through B73 shoot apex hybridized with *GLU1* antisense RNA probe. Arrowhead indicates adaxial accumulation in ligule/auricle region (bar, 200 μm). (g) Longitudinal section through *lg1-R* shoot apex hybridized with *GLU1* antisense RNA probe. No adaxial *GLU1* transcript accumulation detected in ligule/auricle region (bar, 200 μm). (f, g) Asterisk, shoot apical meristem (SAM).

target genes (Bolduc *et al.*, 2012). These include *ZmBOPb* and *ZmCUC2* boundary genes. Similarly, *TRU1*, *ZmBOPa*, *ZHD15*, *ZHD3* and *ZHD21* group with 76 co-expressed genes in a module, suggesting there are genetic interactions between *ZHD* and *BOP* genes.

A co-expression module of 270 genes comprises genes expressed in P6–P7 primordia, including the ligule/auricle patterning genes *LG1*, *LG2* and *ZmRAVL1*, a direct target of LG1 (Tian *et al.*, 2019; Fig. 4a). A nearby, interconnected co-expression module of 184 genes contains the *LG1* and *LG2* paralogs, *SISTER OF LG1* (*SLG1*) and *LG RELATED SEQUENCE1* (*LRS1*), *DEHYDRIN13* (*DHN13*), and *BETA GLUCOSIDASE1* (*GLU1*). *SLG1* is a candidate gene underlying a quantitative trait locus (QTL) for tassel branch angle; this phenotype suggests functional redundancy with LG1, which is a regulator of tassel branch angle (Wu *et al.*, 2016). Moreover, *LRS1* was recently described as a candidate gene underlying a leaf angle QTL, suggesting a potential role in ligule/auricle development (Dzievit *et al.*, 2018). *In situ* hybridization analyses of *DHN13* and *GLU1* showed transcript accumulation specifically in the emerging ligule and preligule band (Fig. 4b–e). Furthermore, *GLU1* transcripts are not detected in the ligule region of *lg1-R* mutants, suggesting that *GLU1* expression requires LG1 function (Fig. 4f,g).

Together, these data suggest that ligule/auricle outgrowth during late (P6–P8) stages of blade–sheath boundary development is associated with the closely connected co-expression modules containing *LG1*, *LG2*, *ZmRAVL1* and related genes. Interestingly, the module that includes *KNOXs*, *ZHDs*, *CUC2* and *ZmBOPs* contains genes that comprise a transcriptional gradient in proximal P4 microdomains (Fig. 2), although many of these genes are *also* expressed later during ligule initiation at P6–P7 (Johnston *et al.*, 2014). Although this module is topologically distant from the co-expression modules containing *LG1*, *LG2* and *RAVL1* implicated in ligule outgrowth (Fig. 4a), these early and late modules are indirectly connected via intermediates such as *IG1*, which is also expressed in P4 and P6–P7 (Fig. 3h–j; Evans, 2007; Johnston *et al.*, 2014). These data suggest a model whereby early-acting coexpression modules generate transcriptional gradients that create a proximodistal prepattern in P4 leaf primordia. Subsequently, later-staged expression modules elaborate the blade/sheath boundary in P6–P7 primordia, reactivating expression of many of the same genes utilized in proximal P4 microdomains.

A common theme in plant and animal development is the utilization of a given gene regulatory network during several ontogenetic stages, from embryogenesis to adulthood and from vegetative to floral development (reviewed by Gilbert, 2010). Examples are also described for networks that function during both early and later stages of organ development. For instance, *CYCLOIDEA* (*CYC*) encodes a transcriptional factor that suppresses abaxial petal initiation early in the development of bilaterally symmetric snapdragon flowers (Luo *et al.*, 1996). Intriguingly, later in petal ontogeny CYC suppresses growth of the dorsal domain of elaborated abaxial petals, giving rise to individual petals that are internally asymmetric.

The concept of prepatterned boundaries formed by transcriptomic gradients within morphologically indistinct developmental fields, followed by the refined localization and elaboration of specific boundary structures later in organ development, can be investigated as a universal mechanism for patterning of developmental boundaries throughout ontogeny. Transcriptomic network analyses, as presented here, are foundational and will enable future genetic, proteomic, metabolomic and other network comparisons that can be integrated to explain molecular mechanisms of development. In particular, this study provides a rich resource of candidate genes for reverse genetic analyses and investigations of protein–protein and protein–DNA interactions during proximodistal patterning of maize leaves.

Acknowledgements

We are grateful to Sarah Hake for her support throughout this study. We thank Erik Vollbrecht, Michael Muszynski, Marty Sachs and the Maize Genetics Cooperative Stock Center for providing genetic stocks. China Lunde, Don Merch and Holly Steinkraus are acknowledged for their help with winter nurseries, as are Kevin Ahern, Nick Lepak and Nick Kaczmar for assisting with planting summer nurseries. We appreciate help from Paul Stachowski for field management, Greg Inzinna and Jerrie Haines for glasshouse plant care and Alicia Corella and Elissa Palmer for growth chamber plant care. We are grateful to Annis Richardson for insightful discussions throughout this project. This research was supported by a National Science Foundation grant to AWS, MJS and Sarah Hake (DEB-1457070, and National Science Foundation Postdoctoral Research Fellowship in Biology grants to JS (IOS-1710973) and SL (IOS-1612268).

Author contributions

RJ, AWS and MJS planned and designed the research. RJ, SF, SL and JS performed experiments and analyzed data. RJ, SL, JS, AWS and MJS wrote the manuscript. RJ, SL and JS contributed equally to this work.

ORCID

Silvia Federici https://orcid.org/0000-0003-4448-4345
Robyn Johnston https://orcid.org/0000-0003-0404-656X
Samuel Leiboff https://orcid.org/0000-0002-6623-1181
Michael J. Scanlon https://orcid.org/0000-0003-1708-3490
Josh Strable https://orcid.org/0000-0002-0260-8285
Anne W. Sylvester https://orcid.org/0000-0001-7282-4189

References

Anders S, Huber W. 2012. *Differential expression of RNA-seq data at the gene level–the DESeq package.* Heidelberg, Germany: European Molecular Biology Laboratory (EMBL). https://pdfs.semanticscholar.org/6262/6783bba72d2bec4ec3424baf7dca7f8416bf.pdf.

Anders S, Pyl PT, Huber W. 2015. HTSeq – a Python framework to work with high-throughput sequencing data. *Bioinformatics* **31**: 166–169.

Andrews S. 2010. *FastQC: a quality control tool for high throughput sequence data.* [WWW document] URL http://www.bioinformatics.babraham.ac.uk/projects/fastqc/.

Becraft PW, Freeling M. 1994. Genetic analysis of *Rough sheath1* developmental mutants of maize. *Genetics* **136**: 295–311.

Bolduc N, Hake S. 2009. The maize transcription factor KNOTTED1 directly regulates the gibberellin catabolism gene *ga2ox1*. *Plant Cell* **21**: 1647–1658.

Bolduc N, O'Connor D, Moon J, Lewis M, Hake S. 2012a. How to pattern a leaf. *Cold Spring Harbor Symposia on Quantitative Biology* **77**: 47–51.

Bolduc N, Yilmaz A, Mejia-Guerra MK, Morohashi K, O'Connor D, Grotewold E, Hake S. 2012b. Unraveling the KNOTTED1 regulatory network in maize meristems. *Genes & Development* **26**: 1685–1690.

Bolger AM, Lohse M, Usadel B. 2014. Trimmomatic: a flexible trimmer for Illumina sequence data. *Bioinformatics* **30**: 2114–2120.

Conklin PA, Strable J, Li S, Scanlon MJ. 2019. On the mechanisms of development in monocot and dicot leaves. *New Phytologist* **221**: 706–724.

Dong Z, Li W, Unger-Wallace E, Yang J, Vollbrecht E, Chuck G. 2017. Ideal crop plant architecture is mediated by *tassels replace upper ears1*, a BTB/POZ ankyrin repeat gene directly targeted by TEOSINTE BRANCHED1. *Proceedings of the National Academy of Sciences, USA* **114**: E8656–E8664.

Dzievit MJ, Li X, Yu J. 2018. Dissection of leaf angle variation in maize through genetic mapping and meta-analysis. *Plant Genome* **12**: 180024.

Erickson RO, Michelini FJ. 1957. The plastochron index. *American Journal of Botany* **44**: 297–305.

Evans MM. 2007. The *indeterminate gametophyte1* gene of maize encodes a LOB domain protein required for embryo sac and leaf development. *Plant Cell* **19**: 46–62.

Ewels P, Magnusson M, Lundin S, Käller M. 2016. MultiQC: summarize analysis results for multiple tools and samples in a single report. *Bioinformatics* **32**: 3047–3048.

Foster T, Yamaguchi J, Wong BC, Veit B, Hake S. 1999. *Gnarley1* is a dominant mutation in the knox4 homeobox gene affecting cell shape and identity. *Plant Cell* **11**: 1239–1252.

Freeling M, Hake S. 1985. Developmental genetics of mutants that specify Knotted leaves in maize. *Genetics* **111**: 617–634.

Gilbert SF. 2010. *Developmental Biology, 9th edn.* Sunderland, MA, USA: Sinauer Associates.

Hepworth R, Pautot VA. 2015. Beyond the divide: boundaries for patterning and stem cell regulation in plants. *Frontiers Plant Science* **6**: 1052.

Hu W, dePamphilis CW, Ma H. 2008. Phylogenetic analysis of the plant-specific *zinc finger-homeobox* and *mini zinc finger* gene families. *Journal of Integrative Plant Biology* **50**: 1031–1045.

Iwakawa H, Ueno Y, Semiarti E, Onouchi H, Kojima S, Tsukaya H, Hasebe M, Soma T, Ikezaki M, Machida C *et al.* 2002. The *ASYMMETRIC LEAVES2* gene of *Arabidopsis thaliana*, required for formation of a symmetric flat leaf lamina, encodes a member of a novel family of proteins characterized by cysteine repeats and a leucine zipper. *Plant and Cell Physiology* **43**: 467–478.

Jackson D. 2002. Double labeling of KNOTTED1 mRNA and protein reveals multiple potential sites of protein trafficking in the shoot apex. *Plant Physiology* **129**: 1423–1429.

Jackson D, Veit B, Hake S. 1994. Expression of the maize KNOTTED-1 related homeobox genes in the shoot apical meristem predicts patterns of morphogenesis in the vegetative shoot. *Development* **120**: 405–413.

Johnston RM, Sylvester AW, Scanlon MJ. 2017. Experimental design for laser microdissection RNA-seq: lessons from an analysis of maize leaf development. *Journal of Visualized Experiments* **121**: doi: 10.3791/55004.

Johnston R, Wang M, Sun Q, Sylvester AW, Hake S, Scanlon MJ. 2014. Transcriptomic analyses indicate that maize ligule development recapitulates gene expression patterns that occur during lateral organ initiation. *Plant Cell* **26**: 4718–4732.

Jun J, Ha H, Fletcher JC. 2010. *BLADE-ON-PETIOLE1* coordinates organ determinacy and axial polarity in Arabidopsis by directly activating *ASYMMETRIC LEAVES2*. *Plant Cell* **22**: 62–76.

Kim D, Pertea G, Trapnel C, Pimental H, Kelley R, Salzberg SL. 2013. TopHat2: accurate alignment of transcriptomes in the presence of insertions, deletions and gene fusions. *Genome Biology* **14**: R36.

Kong F, Zhang T, Liu J, Heng S, Shi Q, Zhang H, Wang Z, Ge L, Li P, Lu X *et al.* 2017. Regulation of leaf angle by auricle development in maize. *Molecular Plant* **10**: 516–519.

Langfelder P, Horvath S. 2008. WGCNA: an R package for weighted correlation network analysis. *BMC Bioinformatics* **9**: 559.

Langfelder P, Horvath S. 2012. Fast R functions for robust correlations and hierarchical clustering. *Journal of Statistical Software* **46**: 1–17.

Lim B, Levine M, Yamazaki Y. 2017. Transcriptional pre-patterning of Drosophila gastrulation. *Current Biology* **27**: 286–290.

Lodha M, Marco CF, Timmermans MCP. 2013. The ASYMMETRIC LEAVES complex maintains repression of *KNOX* homeobox genes via direct recruitment of Polycomb-repressive complex2. *Genes & Development* **27**: 596–601.

Long JA, Moan EI, Medford JI, Barton MK. 1996. A member of the KNOTTED class of homeodomain proteins encoded by the *STM* gene of Arabidopsis. *Nature* **379**: 66–69.

Luo D, Carpenter R, Vincent C, Copsey L, Coen E. 1996. Origin of floral asymmetry in *Antirrhinum*. *Nature* **383**: 794–799.

McCarthy DJ, Chen Y, Smyth GK. 2012. Differential expression analysis of multifactor RNA-Seq experiments with respect to biological variation. *Nucleic Acids Research* **40**: 4288–4297.

Moreno MA, Harper LC, Krueger RW, Dellaporta SL, Freeling M. 1997. *Liguleless1* encodes a nuclear-localized protein required for induction of ligules and auricles during maize leaf organogenesis. *Genes & Development* **11**: 616–628.

Muehlbauer GJ, Fowler JE, Freeling M. 1997. Sectors expressing the homeobox gene *liguleless3* implicate a time-dependent mechanism for cell fate acquisition along the proximal–distal axis of the maize leaf. *Development* **124**: 5097–5106.

Muehlbauer GJ, Fowler JE, Girard L, Tyers R, Harper L, Freeling M. 1999. Ectopic expression of the maize homeobox gene *Liguleless3* alters cell fates in the leaf. *Plant Physiology* **119**: 651–662.

Poethig RS. 1984. Cellular parameters of leaf morphogenesis in maize and tobacco. In: White RA, Dickinson WC, eds. *Contemporary problems of plant anatomy*. New York, NY, USA: Academic Press, 235–259.

Poethig RS, Szymkowiak EJ. 1995. Clonal analysis of leaf development in maize. *Maydica* **40**: 67–76.

Ramirez J, Bolduc N, Lisch D, Hake S. 2009. Distal expression of *knotted1* in maize leaves leads to reestablishment of proximal/distal patterning and leaf dissection. *Plant Physiology* **151**: 1878–1888.

Ritchie ME, Phipson B, Wu D, Hu Y, Law CW, Shi W, Smyth GK. 2015. *limma* powers differential expression analyses for RNA-sequencing and microarray studies. *Nucleic Acids Research* **43**: e47.

Robinson MD, McCarthy DJ, Smyth GK. 2010. edgeR: a Bioconductor package for differential expression analysis of digital gene expression data. *Bioinformatics* **26**: 139–140.

Ruzin SE. 1999. *Plant microtechnique and microscopy*. Oxford, UK. Oxford University Press.

Schneeberger RG, Becraft PW, Hake S, Freeling M. 1995. Ectopic expression of the *knox* homeobox gene *rough sheath1* alters cell fate in the maize leaf. *Genes & Development* **9**: 2292–2304.

Shannon P, Markiel A, Ozier O, Baliga NS, Wang JT, Ramage D, Amin N, Schwikowski B, Ideker T. 2003. Cytoscape: a software environment for integrated models of biomolecular interaction networks. *Genome Research* **13**: 2498–2504.

Smith LG, Greene B, Veit B, Hake S. 1992. A dominant mutation in the maize homeobox gene, Knotted-1, causes its ectopic expression in leaf cells with altered fates. *Development* **11**: 21–30.

Sylvester AW, Cande WZ, Freeling M. 1990. Division and differentiation during normal and liguleless-1 maize leaf development. *Development* **110**: 985–1000.

Tan QKG, Irish VF. 2006. The Arabidopsis *Zinc Finger-Homeodomain* genes encode proteins with unique biochemical properties that are coordinately expressed during floral development. *Plant Physiology* **140**: 1095–1108.

Tian F, Bradbury PJ, Brown PJ, Hung H, Sun Q, Flint-Garcia S, Rocheford TR, McMullen MD, Holland JB, Buckler ES. 2011. Genome-wide association study of leaf architecture in the maize nested association mapping population. *Nature Genetics* **43**: 159–162.

Tian J, Wang C, Xia J, Wu L, Xu G, Wu W, Li D, Qin W, Han X, Chen Q *et al.* 2019. Teosinte ligule allele narrows plant architecture and enhances high-density maize yields. *Science* **365**: 658–664.

Van Norman JM, Xuan W, Beeckman T, Benfey PF. 2013. To branch or not to branch: the role of pre-patterning in lateral root formation. *Development* **140**: 4301–4310.

Walsh J, Waters CA, Freeling M. 1998. The maize gene *liguleless2* encodes a basic leucine zipper protein involved in the establishment of the leaf blade-sheath boundary. *Genes & Development* **12**: 208–218.

Wehrens R, Buydens L. 2007. Self- and super-organizing maps in R: the kohonen package. *Journal of Statistical Software* **21**: 1–19.

Wehrens R, Kruisselbrink J. 2018. Flexible self-organizing maps in kohonen 3.0. *Journal of Statistical Software* **87**: 1–18.

Wu X, Li Y, Shi Y, Song Y, Zhang D, Li C, Buckler ES, Li Y, Zhang Z, Wang T. 2016. Joint-linkage mapping and GWAS reveal extensive genetic loci that regulate male inflorescence size in maize. *Plant Biotechnology Journal* **14**: 1551–1562.

Supporting Information

Additional Supporting Information may be found online in the Supporting Information section at the end of the article.

Dataset S1 The 1984 DEGs identified in P4 microdomains A–E.

Dataset S2 Pairwise differential expression of A and B vs C and D P4 microdomains.

Dataset S3 Pairwise differential expression of A and C vs B and D P4 microdomains.

Dataset S4 Pairwise differential expression of A vs B P4 microdomains.

Dataset S5 Pairwise differential expression of B vs C P4 microdomains.

Dataset S6 Pairwise differential expression of C vs D P4 microdomains.

Dataset S7 Pairwise differential expression of D vs E P4 microdomains.

Dataset S8 Unique differential expression of A vs B amongst neighboring P4 microdomains.

Dataset S9 Unique differential expression of B vs C amongst neighboring P4 microdomains.

Dataset S10 Unique differential expression of C vs D amongst neighboring P4 microdomains.

Dataset S11 Unique differential expression of D vs E amongst neighboring P4 microdomains.

Dataset S12 The 1045 DEGs identified in P4 microdomains A–D.

Dataset S13 Genes strictly upregulated in microdomains A and B.

Dataset S14 Genes strictly upregulated in microdomains C and D.

Dataset S15 Transcription factor DEGs in P4 microdomains A–D.

Dataset S16 P4 DEGs shared with KN1-bound and modulated genes.

Dataset S17 The 23 912 classified gene transcripts used to build the WGCNA.

Fig. S1 Details of laser microdissection of P4 microdomains.

Fig. S2 Laser microdissection of leaf domains from the *liguless2* mutant and wild-type sibling seedlings.

Fig. S3 P4 primordia RNAseq quality control.

Fig. S4 KN1 targets *ZHD* loci.

Fig. S5 KN1 targets *TRU1*/*TRL*/*ZmBOP* loci.

Please note: Wiley Blackwell are not responsible for the content or functionality of any Supporting Information supplied by the authors. Any queries (other than missing material) should be directed to the *New Phytologist* Central Office.